THE JOURNAL OF PHYSICAL CHEMISTRY C
A JOURNAL OF THE AMERICAN CHEMICAL SOCIETY

pubs.acs.org/JPCC

Perspective

Emerging Methods for Controlling Hot Carrier Excitation and Emission Distributions in Nanoplasmonic Systems

Published as part of The Journal of Physical Chemistry virtual special issue "Honoring Michael R. Berman".

Jacob Pettine* and David J. Nesbitt*

Cite This: *J. Phys. Chem. C* 2022, 126, 14767−14780

Read Online

ACCESS | Metrics & More | Article Recommendations

ABSTRACT: Concentrated optical fields in plasmonic metal nanostructures generate high densities of excited charge carriers, which can be extracted or emitted into surrounding media for a variety of physical, chemical, and biological applications. However, the detailed geometry- and field-dependent photoexcitation mechanisms determining the spatial, temporal, vector momentum, and energy distributions of these carriers in nanoplasmonic systems are still under investigation. Gathering insights from recent studies with nanoscale spatial, femtosecond temporal, and/or angle-resolved momentum resolution, we survey several emerging methods for geometrical design and active optical control of nanoplasmonic hot carrier excitation and emission distributions. Uniform dielectric coatings, for example, provide a means of blocking or regulating hot carrier emission, while nonuniform coatings can provide nanoscale spatial selectivity. Nanoscale site selectivity can also be actively controlled on ultrafast time scales by optically addressing different polarization- and/or frequency-sensitive hot spots, particularly with sharp nanocathode geometries such as nanostars. Furthermore, the nanoplasmonic geometry and the corresponding internal vs surface electric field distributions significantly influence the fundamental bulk- vs surface-like photoexcitation mechanisms, with dramatic effects on the excited carrier distributions and dynamics. Finally, energy-resolved pump−probe photoemission studies clarify the tens-of-femtosecond time scales relevant for hot carrier extraction.

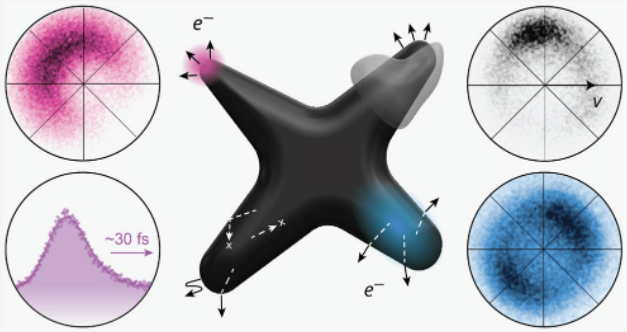

INTRODUCTION

Efficient conversion of optical energy into electronic excitations in nanoplasmonic systems has opened up a variety of new pathways in recent years for product-selective photocatalysis,[1−5] broadband photovoltaics,[6−9] targeted biotherapeutics,[10] ultrafast integrated optoelectronics,[11−13] and highly coherent nanocathodes.[14−17] Plasmonic metal systems, including a wide selection of finely tuned synthetic particles[18−20] and effectively arbitrary nanolithographic structures,[6,11,12,17,21] offer extraordinary optical field concentration into deeply subwavelength nanoscale volumes, along with geometry-dependent responses to optical polarization,[14,22−24] frequency,[14,22,23] intensity,[17,25] and phase.[11] These strong, nanolocalized plasmonic interactions generate high population densities of "hot" carriers (commonly referring to both electron−electron thermalized and nascent/nonthermal photoexcited carriers) with average excitation energies much greater than k_BT of the metal lattice. Despite the numerous applications that rely on the efficient transfer of these hot carriers into surrounding media (e.g., semiconductors, surface-adsorbed molecules, other metals, or free space), a variety of geometric design and optical control degrees of freedom remain relatively untapped due to challenges in predicting and controlling their nanoscale spatial, femtosecond temporal, and vector momentum distributions. With a growing demand for efficient extraction and versatile control over hot carriers, it is becoming increasingly important to take full advantage of these available design and control degrees of freedom.

A major set of nanoplasmonic applications relies on the efficient separation and transfer of excited charge carriers into nearby materials, such as semiconductors[8,26] or surface adsorbed molecules.[3] Along with photodetection and photovoltaic energy collection, metal−semiconductor Schottky junctions can be utilized for charge filtration, spatially separating hot electron and hot hole distributions in photocatalytic applications.[21] Charge transfer may take place either ballistically, following photo-

Received: May 17, 2022
Revised: August 3, 2022
Published: August 25, 2022

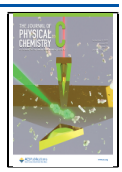

https://doi.org/10.1021/acs.jpcc.2c03425
J. Phys. Chem. C 2022, 126, 14767−14780

excitation throughout the volume of the metal, or directly at the metal−semiconductor[26,27] or metal−molecular interface.[28] In photovoltaic and photocatalytic applications, internal quantum yields for ballistic charge transfer are often less than 1%,[29−34] while enhanced efficiencies have been demonstrated via direct surface photoexcitation.[26,32] In this Perspective, we survey recent work and highlight general design principles for promoting surface- vs bulk-like photoexcitations, while also looking at opportunities to enhance ballistic transfer via tailored hot carrier spatial and momentum distributions.[34] Conversely, we also examine opportunities for blocking or regulating hot carrier transfer with thin dielectric coatings,[35] which can be utilized to eliminate unwanted chemical transformations in surface/tip-enhanced Raman spectroscopy[36] or to distinguish between carrier-induced and thermal effects in plasmon-enhanced photocatalysis, which remains a subject of some debate.[37−39]

Another broad set of emerging nanoplasmonic applications relies on both the efficient ultrafast generation and emission of photoexcited electrons into free space, with tailored kinetic energy and vector momentum distributions. These applications involve either perturbative multiphoton photoemission, thermionic emission, strong-field tunneling emission, or some combination thereof to overcome 4−5 eV metal work functions with visible excitation photon energies in the 1.5−3.1 eV range. When emitted from few-nanometer sources by femtosecond laser pulses, these photoelectron beams can exhibit a high degree of spatiotemporal coherence, which is necessary for imaging ultrafast nanoscale structural or chemical dynamics with techniques such as ultrafast transmission electron microscopy,[40] low-energy electron diffraction,[41−44] or point projection microscopy.[15,16,42] While such techniques currently favor laser-triggered etched nanotip emitters held and manipulated by their macroscopic shanks, the fully nanoscale dimensions of localized plasmonic nanocathodes invite new, integrated schemes for probing the structure and dynamics of nearby nanoscale objects. The high brightness of nanoplasmonic emitters (and arrays thereof) have also attracted interest as pulsed electron sources for X-ray free electron laser systems.[45,46] In addition to their excellent qualities for electron beam sources, plasmonic nanocathodes have demonstrated great promise for carrier-envelope phase-sensitive devices[11,47,48] and terahertz nanoelectronic diodes,[12,49] toward ultrafast information processing and quantum nanophotonic signal transduction.

Predictive understanding of how and where hot carriers are generated, along with their corresponding energy distributions, lifetimes, vector momenta distributions, and transfer efficiencies are clearly essential for progress in many of these nanoplasmonic application areas. In this Perspective, we highlight several recent methods for geometrically designing and actively optically controlling hot carrier distributions and ultrafast dynamics in nanoplasmonic systems (Figure 1), including by means of (i) dielectric or semiconductor coatings, (ii) selective surface hot spot excitation, and (iii) bulk vs surface photoexcitation. Finally, we look at progress in directly probing the ultrafast dynamics of hot carriers in nanoplasmonic systems for insight into the relevant decay mechanisms and extraction time scales. Guided by new measurement techniques and corresponding developments in theoretical modeling, these methods facilitate the optimal design of cocatalyst and filter coatings in site-selective nanocatalysis,[21,50,51] optimization of ballistic and direct excitation/transfer in photocatalysis, photovoltaics, and photodetection,[34,52] and even adaptive spatiotemporal control[53] of ultrafast photoelectron waveforms for nanoelectronics and ultrafast electron imaging.

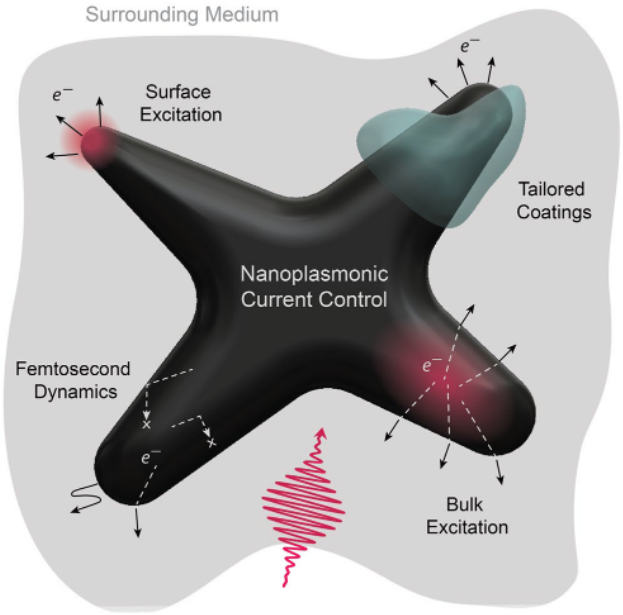

Figure 1. Summary of several emerging methods for controlling nanoscale hot carrier distributions and photocurrents in plasmonic systems.

TAILORING HOT CARRIER EMISSION WITH BESPOKE COATINGS

Perhaps the most conceptually straightforward method of tailoring nanoplasmonic photocurrent distributions is utilizing nonuniform dielectric or semiconductor coatings to block or selectively collect hot carriers, respectively. Insulators such as SiO_2 have long been used to block charge transfer in semiconductor devices, with the wide bandgaps serving as barriers to low-energy carriers around the metal Fermi level or semiconductor conduction band edge. Even hot electrons in plasmonic applications with sufficient energy to transfer into the SiO_2 conduction band (∼3.5 eV above the Au Fermi level), for instance, will travel only a few nanometers before decaying below the escape barrier.[35,54] Thus, dielectric coatings can serve to block photocurrents over a wide range of excitation energies. By contrast, semiconductor coatings are often utilized as energy filters, with lower-energy Schottky barriers (∼1.1 eV for an Au-TiO_2 junction[8]) that can selectively transmit hot electron or hot hole photocurrents.[8,21,55] These are particularly useful for charge separation in nanocatalysis[56] and photovoltaic energy harvesting.[8] Anisotropic coatings also allow for oxidation and reduction to occur at different sites of the nanoparticle, enabling different filters/cocatalysts and facilitating nanoparticle reneutralization for efficient operation.[21,51] Indeed, implicit in all discussions of hot electron (hole) extraction is the need for a complete circuit in which the metal is reneutralized via hole (electron) reinjection. The ideal case is that in which the energy contained within both the hot electron and the hot hole distributions is collected; otherwise, half of the absorbed photon energy may be wasted. The ability to design such systems, particularly for photochemical applications, is greatly facilitated by anisotropic coatings.[21]

https://doi.org/10.1021/acs.jpcc.2c03425
J. Phys. Chem. C 2022, 126, 14767−14780

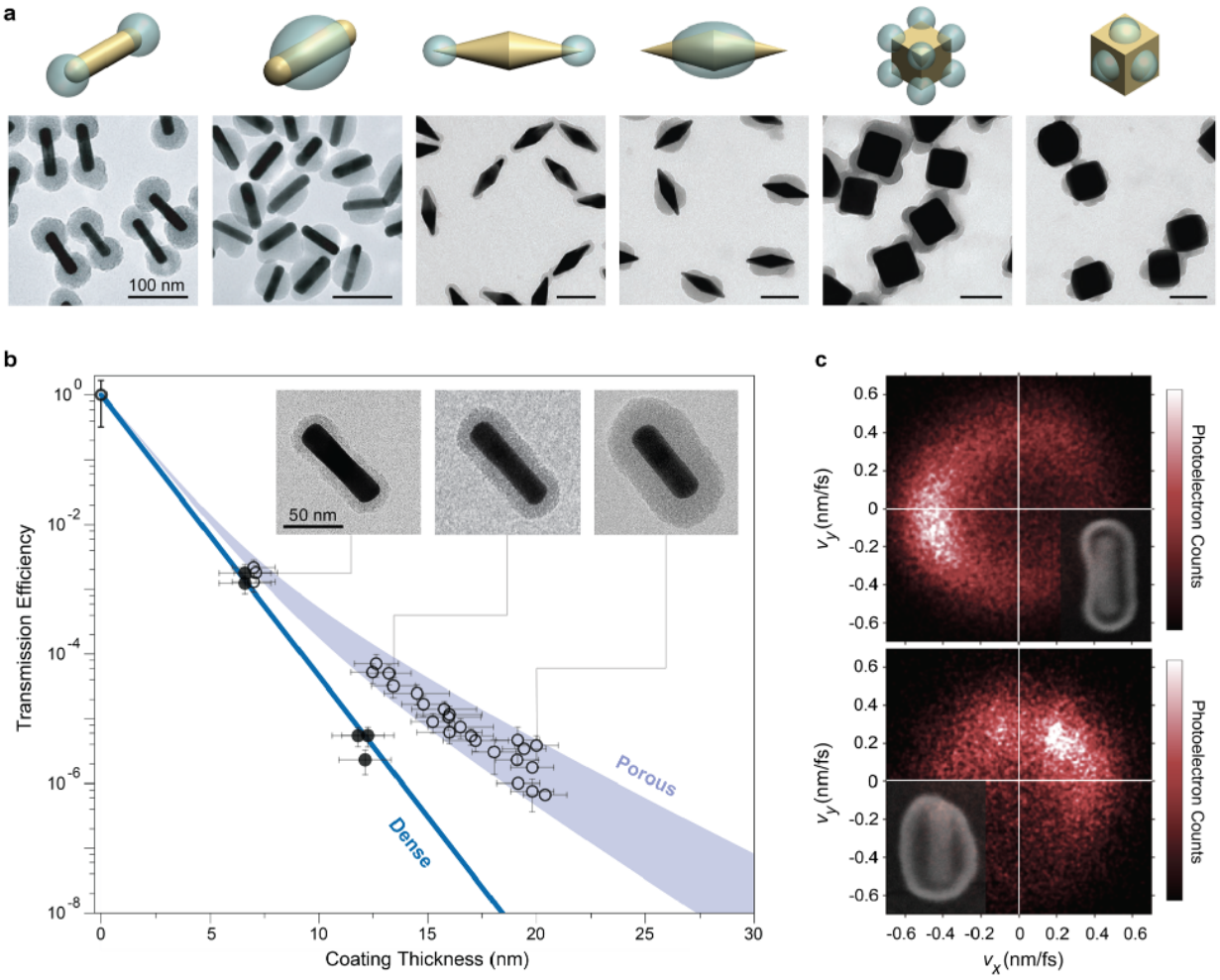

Figure 2. Dielectric coatings for photocurrent or charge transfer regulation and angular control. (a) Examples of gold nanorods, bipyramids, and nanocubes with anisotropic mesoporous silica coatings on the tips or sides. (b) Photoelectron transmission efficiency as a function of uniform dense versus mesoporous silica coating thickness. The single-exponential decay for the dense silica coating occurs with 1 nm effective decay length (blue line), while the nonexponential behavior and increased transmission through the porous silica can be explained in terms of transmission through the randomly aligned pores. Geometrical model shown in light blue with uncertainty bounds on the pore/silica volume ratio of 0.49 ± 0.05. (c) Directional photocurrents emitted through thinner defect regions of silica coatings, demonstrating opportunities for angular photocurrent control and nanoscale site selectivity with tailored anisotropic coatings. Adapted with permission from ref 57 for nanorods in (a). Copyright 2013 Wiley-VCH. Adapted with permission from ref 58 for bipyramids and nanocubes in (a). Copyright 2017 Wiley-VCH. Adapted with permission from ref 35 for (b) and (c). Copyright 2022 American Chemical Society.

Only recently, however, has the design of nonuniform nanoparticle coatings with tens-of-nanometer or better spatial precision become feasible. Along with increasingly precise and versatile nanofabrication capabilities,[21] synthetic techniques have emerged in the past decade that enable controlled anisotropic metal, semiconductor (e.g., TiO_2), dielectric (e.g., SiO_2), and other coatings on metal nanoparticles (Figure 2a),[19,21,51,57−63] as reviewed recently.[64] In many cases these synthetic techniques for anisotropic coatings take advantage of the reduced density of ligands such as cetyltrimethylammonium bromide (CTAB) in regions of high nanoparticle curvature[59] to either (i) selectively grow the desired coatings in these regions,[51,57] or (ii) bind larger ligands that prevent further growth, thereby promoting growth in other surface regions in subsequent coating steps.[19,57]

Both dense and mesoporous silica coatings are commonly used to stabilize nanoparticles in solution while providing increased morphological photostability,[65,66] with mesoporous silica additionally providing channels for size-filtered molecular access to the metal surface.[67] Uniform dense or mesoporous silica coatings can be used to regulate the rate of hot carrier transfer, with few- to tens-of-nanometer thick layers leading to orders-of-magnitude attenuation (Figure 2b). This attenuation can be utilized to block unwanted hot carrier-triggered chemical transformations in surface-enhanced Raman spectroscopy[36] and other plasmon-enhanced photonic applications. Furthermore, silica coatings may also be exploited to quantify the roles of hot carrier vs thermal contributions in nanocatalysis and biotherapeutics (e.g., light-triggered DNA release[10,68]) by blocking charge transfer while still allowing for efficient thermal coupling. Nonuniform coatings, on the other hand, can be utilized to promote charge transfer/emission in controlled nanoscale regions for new site-selective photocatalysis[50] and nanocathode applications.[14]

For any of these applications, however, it is first necessary to understand the hot carrier transmission through uniform dense

https://doi.org/10.1021/acs.jpcc.2c03425
J. Phys. Chem. C 2022, 126, 14767−14780

and mesoporous silica coatings. These studies were performed recently by Medeghini et al.[35] with gold nanorods coated in dense and mesoporous silica coatings of varying thickness. The effective attenuation length of low-energy electrons traveling through the conduction band of SiO_2 (~0−2 eV above the band edge) is remarkably short—approximately 1 nm—due to electron scattering with various phonon modes of the bridging oxygen in the SiO_2 network.[54] This dramatic attenuation behavior is shown in Figure 2b for gold nanorods coated uniformly in dense silica films. In the same study, the transmission dynamics of hot electrons through uniform mesoporous silica coatings were found to differ substantially from dense silica, with much less (though still considerable) attenuation, as well as deviations from single-exponential behavior. A simple geometrical model of transmission through randomly aligned free-space porous channels was introduced to explain these observations, yielding good agreement with the measured transmission efficiencies (Figure 2b).

These basic insights on the dramatic attenuation of hot electron currents through uniform silica coatings illustrate new opportunities for nanoscale spatial control over hot electron transfer/emission distributions with tailored nonuniform coatings. This was also demonstrated recently by Medeghini et al., using photoelectron velocity mapping and correlated scanning electron microscopy to resolve directional emission from thinner defect regions in nominally uniform silica coatings (Figure 2c).[35] The anisotropic coatings influence both nanoscale spatial photocurrent distributions as well as their corresponding vector momentum distributions. Carefully designed synthetic or lithographic coatings could thus be utilized to enhance the directivity of nanocathode emitters (and emitter arrays), influence photocurrent distributions in nanoelectronic systems, or help define nanometer-scale active sites in photocatalytic systems.

SELECTIVE SURFACE HOT SPOTS

Along with the plasmonic enhancement, prolate nanoparticle geometries and sharp nanoparticle features exhibit an extra surface field enhancement factor due to the lightning rod effect.[69,70] The overall electric field enhancement factors of these nanolocalized plasmonic and lightning-rod-enhanced "hot spots" can exceed 50 for some particularly sharp nanoparticle geometries.[14,17,71] Exceptionally strong hot spots with 100-fold or greater field enhancements can even occur in nanoparticle dimer junctions and nanogap plasmons of nanoparticles on conductive substrates,[72−74] as well as within crevice-like surface defects.[24,75,76] While nanoplasmonic hot spots are typically concentrated in surface regions much smaller than the overall emitter surface area, they nevertheless often serve as the dominant excitation/emission source due to the E^2 dependence of linear photoexcitation, with even stronger contributions in nonlinear applications involving multiphoton excitation ($\propto E^{2n}$) or optical field emission.[15,77] Photoemission (or hot electron injection) from highly prolate particles such as nanostars and bipyramids, for instance, is predominantly from the sharp tip hot spots.[4,14,23,78]

Photoexcitation at surface-concentrated hot spots leads to photoelectrons emitted directionally outward in an approximately $\cos\theta$ angular distribution with respect to the surface normal for n-photon photoemission,[14] weighted by the appropriate power of the surface-normal electric field, $E_{\perp}^{2n}$. The photoelectron angular distribution becomes narrower in the strong-field and transitional regimes[79] and is also influenced by postemission surface-normal acceleration due to ponderomotive forces.[17] For sharp, point-like hot spots, both perturbative and strong-field regimes can yield bright photocathode sources[46] with a high degree of spatial coherence and well-defined photocurrent directionality.[14] Photoemission from bound Bloch states into unbound excited states—typically modeled as inverse low-energy electron diffraction (LEED) states[80]—can be calculated via Fermi's golden rule[81] or Green function methods.[82,83] More recent work[79] effectively interpolates between multiphoton photoemission and strong-field regimes and provides a versatile framework for surface photoemission in nanoplasmonics, also yielding good quantitative agreement with recent experiments.[14,84] It should be noted that such surface-mediated photoemission (along with direct interfacial excitation discussed below) generally bypasses hot electron intermediate states.

Advances within the past decade in the synthetic and nanolithographic design of anisotropic nanoparticle and nanostructure geometries have led to new possibilities for optical control via selective excitation of different plasmonic hot spots[23,53,85,86] (Figure 3a,b) and complementary control over photocurrent momentum distributions (Figure 3c).[14,24,87] In the simplest case, different plasmon resonance modes of the same particle or structure lead to separate hot spot excitations, which can be selectively excited via laser polarization, frequency, or carrier-envelope phase. A detailed mapping can then be developed between the multidimensional optical parameter space and the plasmonic hot spot excitations of a system.[85] With the present level of understanding from both spatial- and momentum-resolved studies, hot electron devices are thus primed for adaptive ultrafast control implementations,[53,85,88] as well as application-specific nanoscale geometry optimization via direct and inverse design. The ability to selectively address different plasmonic hot spots on ultrafast time scales leads to the complementary ability to control the photocurrent spatial and vector momentum distributions,[14,89,90] as shown in Figure 3. Such nanoscale control over photocurrents and their directionality has significant implications for optimizing collection in photocatalytic, photovoltaic, and nanoelectronic devices, along with controlling femtosecond nanocathode photoemission distributions for ultrafast electron imaging applications.

SURFACE VERSUS BULK PHOTOEXCITATION

Among other helpful dichotomies, photoexcitation and electron emission processes in nanoplasmonic systems are often framed in terms of ballistic hot carrier transfer from the metal vs direct excitation at the interface (specifically referring to cases with plasmon energies below the energy gap of the interfacial states, such that the charges originate within the metal Fermi sea).[26−28,30,32,91−93] This dichotomy, often discussed for metal−molecule or metal−semiconductor interfaces in nanoplasmonic systems, is closely related to the surface vs bulk paradigm of metal−vacuum interfaces that has been central to the photoemission literature for nearly a century.[83,94−96] Considerable differences in the charge extraction efficiencies and mechanisms will occur for these different systems, particularly for surface-adsorbed molecules, which involve continuum-to-bound or bound-to-bound direct excitations of surface-hybridized molecular orbitals instead of the typical effective continuum-to-continuum free-carrier excitations at vacuum or semiconductor interfaces (neglecting surface/interfacial states). Longer-lived transient ion states and hot electron (or hole) transfer back into the metal can also play a

https://doi.org/10.1021/acs.jpcc.2c03425
J. Phys. Chem. C 2022, 126, 14767−14780

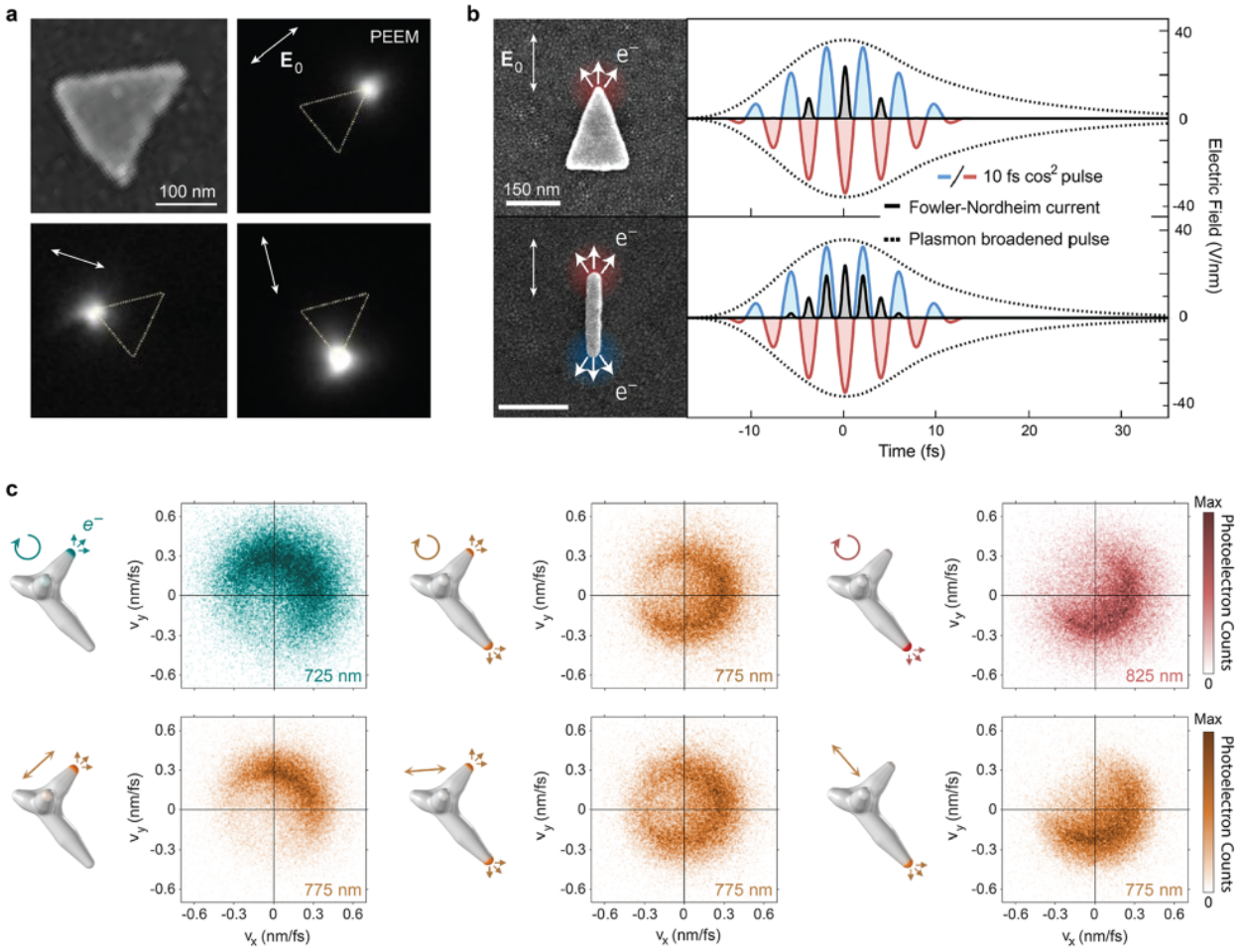

Figure 3. Controlling photoemission by optically addressing different plasmonic hot spots via laser polarization, frequency, and carrier-envelope phase (CEP). (a) Scanning electron micrograph of a representative gold nanotriangle, with photoemission electron microscopy (PEEM) images mapping the photoemission intensity from the three tip hot spots addressed via laser polarization (in-plane projected $\mathbf{E}_0$ indicated). (b) CEP-sensitive optical field emission from a noncentrosymmetric gold nanotriangle and non-CEP-sensitive emission from a centrosymmetric gold nanorod, shown along with the laser field and corresponding calculated Fowler−Nordheim tunneling current over time. (c) Frequency- and polarization-controlled plasmon excitation and hot spot selectivity demonstrated via directional multiphoton photoemission velocity mapping for a single gold nanostar. The frequency dependence is demonstrated with circular polarization at a series of excitation wavelengths from the 725 nm short arm resonance to the 825 nm long arm resonance, while the polarization dependence is demonstrated for different linear polarization axes at 775 nm (directly between the two resonances). Simulated photoemission hot spots are shown for the modeled nanostar geometry. Adapted with permission from ref 86 for (a). Copyright 2012 American Chemical Society. Reprinted with permission from ref 11 for (b). Copyright 2016 Nature Publishing Group. Adapted with permission from ref 14 for (c) Copyright 2020 The Authors (CC BY 4.0).

uniquely important role for photochemical processes.[92] Metal−semiconductor interfaces can also exhibit interfacial states that contribute to excitation and relatively long-lived hot carrier trapping.[27,97] Nevertheless, many of the same underlying principles apply to all of these metal−environment interfaces and we shall proceed to consider new (or rather, old) insights on these important effects in the context of surface vs bulk photoemission, which has been less discussed in the nanoplasmonics context.[30,34]

The surface vs bulk dichotomy is based on the distinction between momentum conservation via surface scattering or bulk scattering mechanisms during photoexcitation, which is of particular interest when considering the spatial and momentum distributions of excited carriers. Surface excitation mechanisms are due to translational symmetry breaking at material interfaces and may include momentum contributions from the electric field discontinuity (enhanced by evanescently decaying plasmonic fields[98]), localized surface states, the exponential internal decay of inverse LEED final states,[80] and/or the few-angstrom exponential external decay of the ground state Bloch wave functions. The transition matrix elements for such surface-mediated excitations depend on the surface-normal component of the electric field, $E_\perp$, with both internal (smaller field but greater electron density) and external (larger field but less electron density) contributions. Bulk mechanisms include interband and intraband excitations, where the latter requires scattering with a third body such as a phonon, defect, or another electron. Bulk excitations do not rely on (but may be influenced by) the presence of an interface, and the transition matrix elements only depend on the total electric field magnitude, E.

Excitation in nanoplasmonic surface hot spots has already been discussed above, but many nanoparticle geometries also exhibit considerable "hot zones" of >10-fold field enhancements within their volumes, which can lead to appreciable volume

https://doi.org/10.1021/acs.jpcc.2c03425
J. Phys. Chem. C 2022, 126, 14767−14780

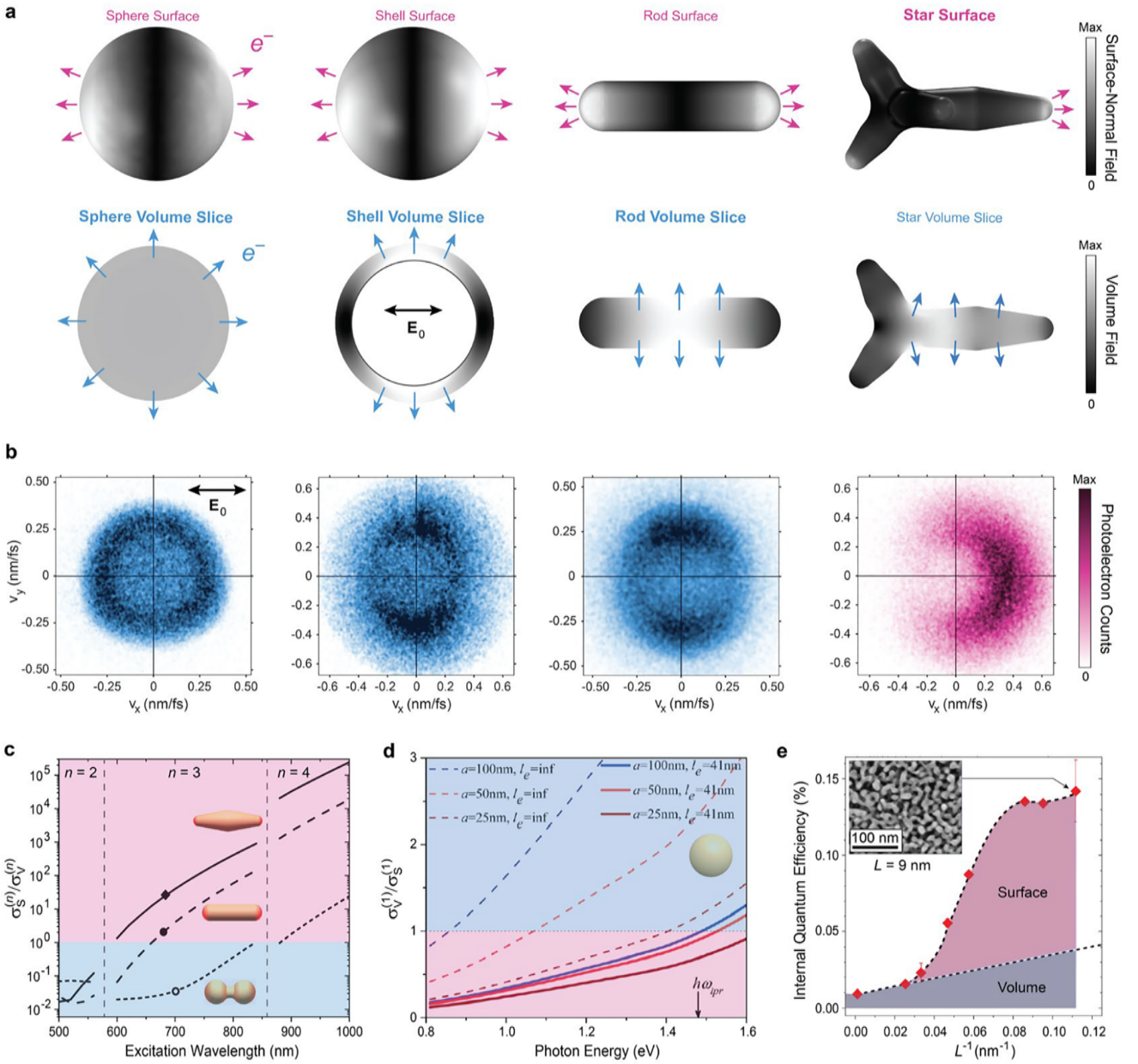

Figure 4. Nanoplasmonic geometry-dependent surface versus bulk photoexcitation/emission. (a) Simulated surface-normal and volume fields for several prototypical gold nanoparticle geometries, with photoemission from surface hot spots and volume hot zones indicated (arrows representing the average direction of the ∼cos θ angular distribution of emission from each surface area element). The incident electric field, $\mathbf{E}_0$, is linearly polarized along the x axis in each case. (b) Measured photoelectron velocity maps from each resonantly excited nanoparticle geometry, with blue indicating predominant volume emission for the sphere (520 nm resonance; 2PPE over ∼4.3 eV escape barrier), shell (650 nm; 3PPE), and rod (750 nm; 3PPE), and magenta representing the predominant surface emission for the star (900 nm; 4PPE). (c) Semiempirical surface/volume n-photon photoemission cross-section ratio, $\sigma_S^{(n)}/\sigma_V^{(n)}$, as a function of excitation wavelength for several gold nanoparticle geometries with different curvatures (bipyramids, rods, and dumbbells) but similar volumes, surface-to-volume ratios, and resonance frequencies (indicated by points). (d) Calculated linear (1PPE) volume/surface internal photoemission (into surrounding semiconductor, 0.8 eV escape barrier) cross-section ratio, $\sigma_V^{(1)}/\sigma_S^{(1)}$, as a function of excitation photon energy for gold nanospheres of different radius (a) and inelastic mean free path (l_e). (e) Measured surface and volume internal quantum efficiencies for 1PPE (291 nm excitation, 3.1 eV escape barrier) into a surrounding electrolyte solution as a function of the inverse average ligament size (L^{-1}) for nanoporous gold films. Adapted with permision from ref 34 for the sphere and rod panels in (b) and for (c). Copyright 2021 American Chemical Society. Adapted with permission from ref 106 for the shell panel in (b). Copyright 2020 American Institute of Physics. Adapted with permission from ref 14 for the star panel in (b). Copyright 2020 The Authors (CC BY 4.0). Adapted with permission from ref 30 for (d) Copyright 2014 Royal Society of Chemistry. Adapted with permission from ref 32 for (e). Copyright 2019 American Chemical Society.

excitation density. Although surface hot spot fields are often much stronger than internal fields due to metallic screening, the different excitation mechanisms and dimensionality for the surface vs bulk necessitate more scrutiny in order to determine which process is dominant. If we approximate spatially independent excitation densities that depend only on the local field intensity, then the dimensionless ratio of surface-to-volume

https://doi.org/10.1021/acs.jpcc.2c03425
J. Phys. Chem. C 2022, 126, 14767−14780

excitation rates for an n^{th}-order (linear $n = 1$ or nonlinear $n > 1$) process can be written generically as

$$\frac{\Gamma_S^{(n)}}{\Gamma_V^{(n)}} = \frac{\rho_S^{(n)} \int E_\perp^{2n}\, \mathrm{d}S}{\rho_V^{(n)} \int E^{2n}\, \mathrm{d}V} \tag{1}$$

The ratio of field-dependent excitation densities, $\rho_S^{(n)}/\rho_V^{(n)} \equiv l_{\mathrm{eff}}^{(n)}$, has units of length and can be thought of as an effective thickness associated with surface excitations, accounting for difference mechanisms contributing to the photoexcitation matrix elements. Note that $l_{\mathrm{eff}}^{(n)}$ should not be confused with the actual spatial extent over which surface excitation occurs, which requires a more careful analysis of the nonlocal material response.[98] Nevertheless, we may rewrite eq 1 as

$$\frac{\Gamma_S^{(n)}}{\Gamma_V^{(n)}} = \frac{\int E_\perp^{2n} (l_{\mathrm{eff}}^{(n)}\, \mathrm{d}S)}{\int E^{2n}\, \mathrm{d}V} \tag{2}$$

A recent photoemission study measured $l_{\mathrm{eff}}^{(3)} \approx 7.5$ pm, and although this value may change significantly for different n and for photoexcitation vs photoemission (in particular, $l_{\mathrm{eff}}^{(n)}$ neglects volume escape efficiencies much smaller than unity[34]), the small size of 7.5 pm compared with the few- to tens-of-nanometer depths over which volume fields typically extend illustrates how bulk photoexcitation can be dominant despite the much greater plasmon-enhanced electric fields in surface hot spots.

Furthermore, volume hot zones are typically spatially distinct from the surface hot spots (Figure 4a) and exhibit very small surface-normal field components with respect to the nearest surfaces. This can be understood in terms of boundary conditions: Surface hot spots correspond to regions of high curvature with a large charge buildup during plasmonic oscillations, leading to strong surface-normal fields that decay evanescently outside of the particle. However, in the typical absence of free charges (i.e., neutral metal nanoparticles), the surface-normal field just within the metal is $|E_{\perp,\mathrm{in}}| = |(\epsilon_0/\epsilon(\omega))E_{\perp,\mathrm{out}}|$, where $|\epsilon_0/\epsilon(\omega)| \approx 0.07$ for a gold−vacuum interface at 700 nm excitation wavelength. This boundary condition ensures a relatively small plasmonic field enhancement in volume regions near surface hot spots, depending on the surrounding medium. However, for nonellipsoidal geometries the nonuniform internal fields can become very large in other regions—see nanoshells, nanorods, and nanostars in Figure 4a—in which the surface-normal component with respect to adjacent surfaces remains small but where surface-parallel fields can be relatively large (with the boundary condition $E_{\parallel,\mathrm{in}} = E_{\parallel,\mathrm{out}}$). As a result, excitation in volume hot zones is often dominated by bulk excitation mechanisms, which are proportional to the *total* field intensity (or E^{2n} for an n-photon process) rather than the surface-normal field intensity. The important takeaway is that, in many nanoplasmonic systems, it becomes both conceptually and practically straightforward to separate bulk-like excitation mechanisms in volume hot zones from surface-like excitations in surface hot spots.

Before proceeding, one exception and a source of some ambiguity for this paradigm should be addressed. Even slight discretization effects in tens-of-nanometer particles can lead to considerable "geometry-assisted" excitation contributions,[99] which have been calculated analytically via Fermi's golden rule in jellium models.[100−103] Such effects are clearly due to the surface boundary conditions and can also be rationalized in terms of surface scattering.[103] However, in spherical particles (in which the internal fields are uniform) the excitation density has been shown to be more or less uniform throughout the volume,[101] which is a bulk-like quality. Thus, while such geometry-assisted transitions serve to break the bulk vs surface paradigm (which completely breaks down at the few-nanometer scale) in principle, it is possible that they may be treated as bulk-like excitations in practice with respect to the relevant hot carrier spatial and momentum distributions. This exception underscores the danger of interpreting helpful dichotomies too rigidly or generally, and highlights the necessity for further experimental investigations into geometry-assisted hot carrier distributions.

Much more can be said and much more remains to be explored on the fundamental aspects of surface- vs bulk-like excitations in nanoscale systems, but henceforth we will restrict our attention to the salient effects of these different excitation mechanisms on hot carrier distributions in real space and momentum space. Whereas surface-excited electrons are emitted directionally outward (on average) from nanolocalized hot spots,[14,15,104] volume-excited hot electrons simply spill out more broadly from all nearby surface areas within an inelastic mean free path of the excitation region.[33,34,105,106] Such behaviors are demonstrated in Figure 4a,b. Bulk dynamics can be modeled as a ballistic three-step process involving (i) local excitation, (ii) transport to the surface with the possibility of elastic or inelastic scattering, and (iii) possible escape over the surface barrier if the surface-normal momentum is sufficient.[107] Along with direct integration of ballistic photoemission models for various analytical geometries (including spheres, ellipsoids, cylinders, and truncated cones),[33,108] the full evolution of hot carrier spatial and momentum distributions can be traced in arbitrary nanoscale geometries via Monte Carlo integration of these models.[34,105,109,110] Such calculations have been performed with varying degrees of detail, including accounting for simulated spatially varying plasmonic field distributions,[34,105] first-principles excitation rates,[105] nonlocality, quasi-elastic electron−phonon scattering in the bulk,[34,105,110] nonlinear excitation,[34] and diffuse and/or specular multiple surface scattering effects.[110] The basic validity of such semiclassical methods has been verified in a recent comparison between momentum-resolved photoemission experiments and ballistic theory.[34]

Unlike bulk excitations, direct excitation at the surface precludes any decay due to inelastic scattering and can lead to more efficient charge transfer (Figure 4e),[32] with internal quantum efficiencies greater than 20% demonstrated for very small (<5 nm) gold nanoparticles attached to CdSe nanorods.[26] Ballistic bulk-like charge transfer, by contrast, exhibits typical efficiencies below 1%,[29−32,111] despite around 50% of the nascent hot electrons having sufficient energy to overcome a typical ∼1 eV Schottky barrier at visible excitation energies. This poor collection efficiency can be attributed to a combination of two factors: (i) Tens-of-nanometer inelastic mean free paths due to electron−electron scattering.[112,113] (ii) Insufficient *surface-normal* momentum to overcome the surface barrier for incidence angles beyond the maximum escape angle (defining the "escape cone"), $\theta_{\mathrm{max}} = \cos^{-1}\sqrt{(\phi + E_F)/(E_e + E_F)} \approx 10°−15°$ for typical excess energies of $E_e - \phi \approx 0.5$ eV, where ϕ is the barrier height (metal−vacuum work function or metal−semiconductor Schottky barrier) and E_e is the hot electron excitation energy (both referenced to the Fermi level, E_F). These fundamental limitations also indicate how ballistic carrier collection efficiencies may be improved, by more careful design of the

https://doi.org/10.1021/acs.jpcc.2c03425
J. Phys. Chem. C 2022, 126, 14767−14780

spatial and momentum distributions with respect to the collection interface following photoexcitation in tailored field-enhanced volume regions. In particular, collection efficiencies may be improved by designing bulk excitation regions well within an inelastic mean free path of the surface, as well as smaller/higher-curvature particle features around these hot zones, possibly also taking advantage of rough surfaces to relax the dependence of collection efficiency on surface-normal momentum.[111] By completely relaxing this requirement and assuming a ballistic model with unity interfacial transmission efficiency for hot electrons with sufficient energy, one study calculated and measured 20−40% internal quantum yields in the visible range for small gold nanoparticles embedded in a TiO_2 matrix.[114] While the mechanism in this study remained unclear and may have been due to some combination of direct surface excitations, multiple surface scattering, and/or surface roughness effects, this underscores the important role of vector-momentum-dependent surface transmission for the collection of ballistic hot carriers.

Beyond opportunities for geometrically *designing* plasmonic fields to promote either surface hot spot emission or volume hot zone emission upon resonant excitation, it is also possible to optically *control* surface vs bulk contributions in at least two ways: (i) frequency- or polarization-selective excitation of different plasmonic modes that promote different mechanisms due to different internal/surface field distributions, or (ii) by frequency-dependent screening effects. With the second method, it has been shown that particles such as nanorods that behave as bulk emitters (transverse emission; Figure 4b) on resonance can transition to surface emitters (longitudinal emission) with sufficient red detuning of the excitation light (Figure 4c,d).[34] This is due to the enhanced screening of the incident radiation within the metal for lower frequencies, which dramatically and disproportionately decreases the volume hot zones relative to the surface hot spots.[34] Indeed, the surface/volume excitation ratio (Figure 4c) essentially follows the trend of $|\epsilon(\omega)/\epsilon_0|^{2n}$ due to the effect of screening on the field integral ratio in eq 1, whereas the frequency dependence of $\rho_S^{(n)}/\rho_V^{(n)}$ is expected to largely cancel out and thus be much less significant.[34] For many nanoplasmonic geometries, this frequency-dependent surface-bulk transition will lead to entirely different spatial distributions of hot electron excitation and momentum distributions of emission, as illustrated in Figure 4a.

As a final remark on this subject, we note that such a high degree of control over both nonuniform volume- and surface-excited hot carrier spatial and momentum distributions is only available in the perturbative single- or multiphoton excitation regimes. By contrast, emission currents in the strong-field regime are necessarily highly localized to surface hot spots, while electron−electron thermalized hot carrier transfer or emission (i.e., thermionic emission) generally leads to a more uniform spilling out of hot carriers from all surfaces. It is intriguing, however, that several recent studies have provided evidence of nonuniform nanoscale thermal distributions and corresponding nonuniform thermionic or thermally assisted emission.[90,115] In the examples provided in Figure 4, the process orders range from $n = 1$ (1PPE) to 4 (4PPE) for different excitation photon energies and escape barriers. While in some cases (excitation energy >2 eV; $\lambda < 620$ nm) d-band interband excitations can become a prominent source of absorption, the excited carriers remain too close to the Fermi level to escape. Thus, in each case shown, intraband excitations are the dominant source of signal, which will indeed remain the case for most plasmon-resonant excitations for and typical escape/transfer barriers >1 eV. The multiphoton intraband excitations can include coherent transitions through virtual intermediate states (no corresponding intermediate state population), incoherent transitions through intermediate eigenstate population, or some mixture thereof, yet plasmon-mediated *n*PPE (particularly for $n > 2$) is often attributed to the coherent channel (though more work is required).[116,117] Despite quantitative differences in transition matrix elements and relative field weighting for these different process orders, many of the general insights discussed here on the surface vs bulk dichotomy can be expected to apply for linear and nonlinear photoexcitation.

■ ULTRAFAST HOT CARRIER DYNAMICS

Thus, far, we have discussed the design and/or active control of nanoscale hot carrier distributions via some combination of nanoparticle (or coating) geometry and the mapping of optical degrees of freedom such as polarization and frequency onto nanoplasmonic electric field distributions, with corresponding influences on surface- and bulk-like photoexcitation distributions. For the most part, these methods for manipulating hot carrier spatial and momentum distributions do not rely on the overall intensity or electron temperature and thus conceptually apply to both ultrafast and continuous wave (CW) excitation, with CW multiphoton photoemission even observed recently at nanostar tip hot spots.[118] However, femtosecond pulsed excitation is clearly essential for efficient nonlinear applications, along with investigations of hot carrier dynamics on their natural femtosecond time scales—also necessary for understanding steady-state distributions and extraction efficiencies under CW excitation. Additionally, pulsed excitation augmented by plasmonic enhancements creates new opportunities for dynamic control of hot carrier distributions and dynamics with tailored ultrafast laser fields,[53,85] along with a variety of strong-field physics.[17,70,89,119,120] In this section, we will consider some recent insights from ultrafast studies of hot carrier dynamics in nanoplasmonic systems, focusing on perturbative rather than strong-field processes. Exciting developments in related areas of nanoplasmonic coherent control on atto- to femtosecond time scales have been covered in detailed recent reviews.[70,120]

Efficient hot carrier extraction to perform useful work in photocatalysis, photovoltaics, integrated optoelectronics, and other applications relies not only on a detailed knowledge of the initial spatial and momentum distributions of photoexcited carriers but also on their subsequent single-particle decay dynamics and overall population kinetics. In bulk and thin film copper, silver, gold, and aluminum, the lifetimes of 0.5−2 eV hot electrons are in the tens-of-femtosecond range and depend strongly on excitation energy.[121] In particular, the lifetimes of these low-energy nearly free electron (quasiparticle) excitations within a few electronvolts of the Fermi level, E_F, approximately follow Fermi liquid theory behavior, with lifetimes $\propto(E - E_F)^{-2}$.[121−123] The primary decay mechanism in these cases is inelastic electron−electron scattering with the "cold" Fermi sea electrons. In nanoscale systems, however, hot carrier dynamics are expected to deviate from bulk-like behaviors. First of all, nanoscale systems (including thin films) limit the effects of ballistic transport out of the excitation region, thus yielding longer lifetimes in thin films compared with artificially shortened lifetimes observed in thick/bulk materials[124] (Figure 5b). However, it has been shown that thermalization times of hot carrier distributions (and thus individual hot carrier lifetimes) decrease with decreasing Ag and Au nanoparticle size (Figure

https://doi.org/10.1021/acs.jpcc.2c03425
J. Phys. Chem. C 2022, 126, 14767−14780

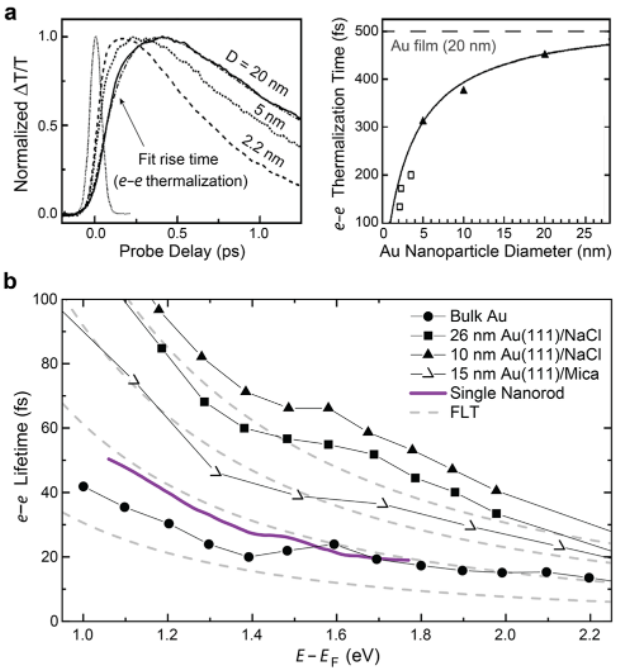

Figure 5. Ultrafast hot carrier dynamics in metal films and nanoparticles. (a) Transient transmission measurements of gold nanoparticle ensembles embedded in a dielectric matrix for 1.32 eV pump photon energy and 3.95 eV probe photon energy, along with a summary of the fit rise (electron−electron thermalization) times as a function of particle diameter compared with 20 nm Au film. These measurements are not energy resolved and thus represent an average of the dynamics over all hot carrier energies. (b) Energy-resolved two-photon photoemission studies of bulk Au, 10 and 26 nm Au(111) on NaCl from ref 124, 15 nm Au(111)/mica from ref 132, and single gold nanorods from ref 130. Fermi liquid theory calculations shown for comparison with a = 1, 2, 3, 4 fs and E_F = 5.53 eV in the general expression, lifetime = $aE_F^2/(E - E_F)^2$. (a) is adapted with permission from ref 126. Copyright 2004 American Physical Society.

5a), due to the local reduction of charge density and reduced screening in the surface region leading to increased interactions.[125,126] For very small (<3 nm) particles there is more at play still, as silver nanoparticle ensembles supported on graphite were shown to exhibit longer lifetimes than typical silver thin films in the >1.5 eV excitation energy range.[127] This has been attributed to quantum confinement in these very small systems and the corresponding reduced density of states and electron−electron interactions.[101,128,129]

Recently, the first energy-resolved femtosecond pump−probe photoemission studies of single nanoparticles have demonstrated bulk-like carrier dynamics (i.e., Fermi liquid theory behavior with bulk-like lifetimes) at application-relevant 1−2 eV excitations energies in gold nanorods with 10 nm diameters (Figure 5b).[130] Angle-resolved photoelectron velocity mapping provided unambiguous evidence of bulk-like photoexcitation and ballistic dynamics, with hot electrons ultimately spilling out of the sides due to the larger surface area compared with the tips and a centralized plasmonic field enhancement (Figure 4a), as also shown recently in single-color multiphoton photoemission studies of single gold nanorods.[34] Furthermore, the hot electron dynamics were found to be insensitive to particle geometry for vastly different 10 nm × 40 nm monocrystalline gold nanorods and 160 nm/120 nm diameter polycrystalline gold shell/silica core nanoshells.[130] These studies were performed with plasmon-coupled 1.8 eV excitation photon energies, just below the ∼2 eV onset of d-band absorption for gold. This precludes several potentially significant complicating effects present in most of the previous gold film studies, which were typically performed at >3 eV excitation photon energy to overcome the ∼5 eV metal work function while measuring dynamics for a broad range of excitation energies. For such excitation photon energies, enhanced d-band excitation and Auger decay effects considerably influence the dynamics.[121,131] Cascading or in-filling from higher energy levels into the <2 eV range also become prominent, leading to longer effective lifetimes.[121] It is thus likely that this effect contributes to the much longer lifetimes measured for Au thin films[132] ($\hbar\omega_{pump}$ = 3.2 eV) compared with Au nanoparticles[130] ($\hbar\omega_{pump}$ = 1.8 eV), summarized in Figure 5b. Variations in lifetimes measured in different experiments with different substrates, sample preparation procedures, and other systematic factors can also be significant, as illustrated for the different Au film studies performed by Cao et al.[132] and Aeschlimann et al.[124] shown in Figure 5b.

These direct time- and energy-resolved two-photon photoemission studies provide insight into the time scales relevant for hot carrier extraction and, when combined with theoretical modeling or experimental resolution on spatial and momentum photoexcitation distributions, suggest guidelines for designing efficient hot carrier collection. This is important given that the much longer hundreds-of-femtosecond energy-averaged hot carrier thermalization times measured in seminal optical pump−probe studies of metal nanoparticles[125,126,133] (Figure 5a) are often invoked as the relevant time scale of hot carrier decay, as featured in the typical sequence of plasmon dephasing (∼1−10 fs), electron−electron thermalization (∼100−500 fs), electron−phonon thermalization (∼1−10 ps), and lattice-environment thermalization (>10 ps) time scales.[129,134,135] While this sequence is generally correct and serves as a helpful guideline, the energy-averaged electron−electron thermalization times measured in optical pump−probe studies are dominated by the much longer decay time scales of low-energy excitations.[125,136] In the ∼1−2 eV excitation energy range relevant to many applications, it is well-known from numerous energy-resolved photoemission pump−probe studies of noble metal bulk, thin films, and nanoparticles discussed above that the hot carrier lifetimes are in the tens-of-femtosecond range (Figure 5b,c)—i.e., about an order of magnitude faster than the overall electron−electron thermalization time.

Furthermore, a simple calculation demonstrates that the nascent hot carriers with fast tens-of-femtosecond decay dynamics are likely to be most relevant for applications involving extraction into/over >1 eV energy levels/barriers, despite the significantly longer (few-picosecond) lifetimes of electron−electron thermalized carriers. To avoid keeping track of carrier multiplication effects due to electron−electron scattering, we make such comparisons in terms of a more relevant quantity, the available energy. In particular, for a population of truly "hot" electrons thermalized via electron−electron scattering over hundreds of femtoseconds following pulsed laser excitation to a Fermi−Dirac distribution at ∼1000 K electron temperature, less than 0.001% of the energy in the hot carrier distribution lies above 1 eV. This is accounting for energy stored in the hot electron and hot hole distributions and may be compared with 30% of the energy in the nascent/nonthermal carrier distribution with 1.55 eV (800 nm) excitation photons. If one reasonably assumes that most/all of the nascent excitation energy is ultimately transferred into the thermal distribution via

https://doi.org/10.1021/acs.jpcc.2c03425
J. Phys. Chem. C 2022, 126, 14767−14780

electron−electron scattering, the nascent distribution contains greater than 30,000 times the available energy above 1 eV. However, we must also consider the fact that thermalized carriers live ∼100 times longer (few-picosecond electron−phonon thermalization times[134]) than the nascent carriers (few tens-of-femtosecond electron−electron decay times) in this >1 eV energy range. Combining these simple estimates yields a 300-fold greater energy availability in the nascent vs thermalized electron distributions, even for *pulsed* laser excitation with a relatively high ∼1000 K electron temperature.

Based on these estimates, electron−electron thermalized hot carrier collection at excitation energies >1 eV only becomes appreciable for >2000 K transient electron temperatures. While such electron temperatures can be achieved with femtosecond pulsed laser excitation, the role of thermalized carriers for CW (including solar) excitation with significantly lower steady-state electron temperatures may be expected to become completely negligible compared with nascent carriers. These arguments also neglect the effects of ballistic collection efficiency, which may be enhanced for tailored nascent excitations (see previous section) compared with thermalized hot carriers that will have already spread throughout the particle and indiscriminately sample the entire surface area. Given these simple arguments, it is clearly essential for many applications to design nanoplasmonic systems that can transfer as many *nascent* carriers as possible, either by (i) direct interfacial excitation or via (ii) bulk generation in field-enhanced regions close to high-curvature (or rough[111]) surfaces to achieve higher average values of surface-normal momentum.

Finally, we note that while much emphasis has been given to hot electron dynamics (here and in general), recent studies have begun to explore ultrafast hot hole dynamics at p-type semiconductor interfaces.[97] These studies by Tagliabue et al. have demonstrated both the influence of long-lived charge trapping interfacial states (lifetimes around ∼10 ps and ∼5 ns) on hot hole extraction, as well as the remarkable effect hot hole collection has on the hot electron dynamics via the electron-density-dependent electronic heat capacity. In particular, it was found that the increased electron density in the gold nanoparticles (as hot holes were transferred away) led to an increase in the electronic heat capacity and corresponding decrease in the peak electron temperature and electron−phonon decay time.[97,134] These studies underscore the need for further emphasis on hot hole dynamics in nanoplasmonic applications, where the hot hole distribution contains at least half of the absorbed photon energy (or more for excitation energies beyond the d-band threshold) and also dynamically influence the hot electron distribution.

SUMMARY

The basic insight that nanoscale light concentration in plasmonic nanoparticles can yield high densities of highly excited charge carriers has stimulated a significant body of research in hot carrier science and technology, even without detailed understanding of the nanoscale distributions and ultrafast dynamics. Recent studies with nanoscale spatial and femtosecond temporal resolution, along with angle-resolved momentum resolution, have further expanded the capabilities and opportunities in this field. Having surveyed several emerging methods for exploiting designer nanoscale geometries and coatings, along with optically controlled photoexcitation and emission distributions, it is clear that many avenues remain to be explored in existing application areas and exciting new areas of nanophotonics and nanoelectronics.

AUTHOR INFORMATION

Corresponding Authors

Jacob Pettine − *Center for Integrated Nanotechnologies, Los Alamos National Laboratory, Los Alamos, New Mexico 87545, United States*; Email: jacob.pettine@lanl.gov

David J. Nesbitt − *JILA, University of Colorado Boulder and the National Institute of Standards and Technology, Boulder, Colorado 80309, United States; Department of Chemistry, University of Colorado Boulder, Boulder, Colorado 80309, United States; Department of Physics, University of Colorado Boulder, Boulder, Colorado 80309, United States*; orcid.org/0000-0001-5365-1120; Email: djn@jila.colorado.edu

Complete contact information is available at: https://pubs.acs.org/10.1021/acs.jpcc.2c03425

Notes

The authors declare no competing financial interest.

Biographies

Jacob Pettine received his Ph.D. in physics as an NSF Graduate Research Fellow at the University of Colorado Boulder and JILA. Working with Prof. David J. Nesbitt, he developed new capabilities for measuring, modeling, and optically controlling ultrafast carrier dynamics in nanoplasmonic systems. As a Director's Postdoctoral Fellow at Los Alamos National Laboratory, he is now utilizing these insights to explore ultrafast nanophotonic and nanoelectronic dynamics in emerging hybrid plasmonic-quantum material systems.

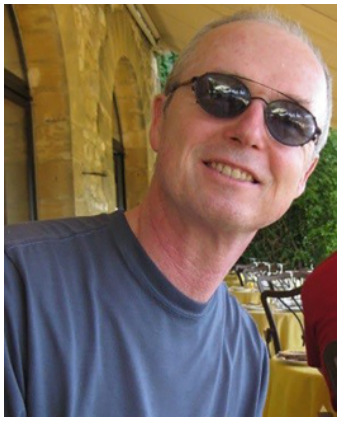

David J. Nesbitt is presently Full Professor Adjoint in the Departments of Chemistry and Physics at the University of Colorado, a Fellow of JILA, and a Physicist in the Quantum Physics Division of the National Institute of Standards and Technology. His experimental research at JILA involves application of direct absorption IR laser techniques to

https://doi.org/10.1021/acs.jpcc.2c03425
J. Phys. Chem. C 2022, 126, 14767−14780

study (i) CW and frequency comb spectroscopy of transient combustion radicals and molecular ions in slit supersonic jet expansions, (ii) quantum state-resolved inelastic/reactive scattering at gas−liquid and gas−solid interfaces, (iii) temperature- and pressure-dependent kinetics/thermodynamics of RNA tertiary folding dynamics by single molecule fluorescence microscopy, and as featured in this Perspective, (iv) ultrafast scanning photoelectron imaging microscopy of plasmonic nanostructures.

■ ACKNOWLEDGMENTS

Many of the photoemission studies described herein have been supported by the Air Force Office of Scientific Research (FA9550-15-1-0090), with additional funds for laser development and apparatus construction provided by the National Science Foundation (PHY-1734006/CHE-2053117). J.P. was supported by the Laboratory Directed Research and Development program of Los Alamos National Laboratory under project number 20210845PRD1 while preparing this Perspective. D.J.N. wishes to thank Michael Berman for his skillful multidecade management of the AFOSR program, his long-standing intellectual support, and indeed the expert leadership and moral encouragement to pursue the remarkable breadth of scientific directions he ultimately made possible.

■ REFERENCES

(1) Zhang, X.; Li, X. Q.; Zhang, D.; Su, N. Q.; Yang, W. T.; Everitt, H. O.; Liu, J. Product Selectivity in Plasmonic Photocatalysis for Carbon Dioxide Hydrogenation. *Nat. Commun.* **2017**, *8*, 14542.

(2) Robatjazi, H.; Zhao, H. Q.; Swearer, D. F.; Hogan, N. J.; Zhou, L. N.; Alabastri, A.; McClain, M. J.; Nordlander, P.; Halas, N. J. Plasmon-Induced Selective Carbon Dioxide Conversion on Earth-Abundant Aluminum-Cuprous Oxide Antenna-Reactor Nanoparticles. *Nat. Commun.* **2017**, *8*, 27.

(3) Cortes, E. Efficiency and Bond Selectivity in Plasmon-Induced Photochemistry. *Adv. Opt. Mater.* **2017**, *5*, 1700191.

(4) Sousa-Castillo, A.; Comesana-Hermo, M.; Rodriguez-Gonzalez, B.; Perez-Lorenzo, M.; Wang, Z. M.; Kong, X. T.; Govorov, A. O.; Correa-Duarte, M. A. Boosting Hot Electron-Driven Photocatalysis through Anisotropic Plasmonic Nanoparticles with Hot Spots in Au-TiO_2 Nanoarchitectures. *J. Phys. Chem. C* **2016**, *120*, 11690−11699.

(5) Christopher, P.; Xin, H. L.; Marimuthu, A.; Linic, S. Singular Characteristics and Unique Chemical Bond Activation Mechanisms of Photocatalytic Reactions on Plasmonic Nanostructures. *Nat. Mater.* **2012**, *11*, 1044−1050.

(6) Knight, M. W.; Sobhani, H.; Nordlander, P.; Halas, N. J. Photodetection with Active Optical Antennas. *Science* **2011**, *332*, 702−704.

(7) Mubeen, S.; Hernandez-Sosa, G.; Moses, D.; Lee, J.; Moskovits, M. Plasmonic Photosensitization of a Wide Band Gap Semiconductor: Converting Plasmons to Charge Carriers. *Nano Lett.* **2011**, *11*, 5548−5552.

(8) Clavero, C. Plasmon-Induced Hot-Electron Generation at Nanoparticle/Metal-Oxide Interfaces for Photovoltaic and Photocatalytic Devices. *Nat. Photonics* **2014**, *8*, 95−103.

(9) Ng, C.; Cadusch, J. J.; Dligatch, S.; Roberts, A.; Davis, T. J.; Mulvaney, P.; Gomez, D. E. Hot Carrier Extraction with Plasmonic Broadband Absorbers. *ACS Nano* **2016**, *10*, 4704−4711.

(10) Goodman, A. M.; Hogan, N. J.; Gottheim, S.; Li, C.; Clare, S. E.; Halas, N. J. Understanding Resonant Light-Triggered DNA Release from Plasmonic Nanoparticles. *ACS Nano* **2017**, *11*, 171−179.

(11) Putnam, W. P.; Hobbs, R. G.; Keathley, P. D.; Berggren, K. K.; Kärtner, F. X. Optical-Field-Controlled Photoemission from Plasmonic Nanoparticles. *Nat. Phys.* **2017**, *13*, 335−339.

(12) Karnetzky, C.; Zimmermann, P.; Trummer, C.; Sierra, C. D.; Wörle, M.; Kienberger, R.; Holleitner, A. Towards Femtosecond on-Chip Electronics Based on Plasmonic Hot Electron Nano-Emitters. *Nat. Commun.* **2018**, *9*, 2471.

(13) Dorodnyy, A.; Salamin, Y.; Ma, P.; Plestina, J. V.; Lassaline, N.; Mikulik, D.; Romero-Gomez, P.; Morral, A. F. I.; Leuthold, J. Plasmonic Photodetectors. *IEEE J. Sel. Top. Quant.* **2018**, *24*, 4600313.

(14) Pettine, J.; Choo, P.; Medeghini, F.; Odom, T. W.; Nesbitt, D. J. Plasmonic Nanostar Photocathodes for Optically-Controlled Directional Currents. *Nat. Commun.* **2020**, *11*, 1367.

(15) Müller, M.; Kravtsov, V.; Paarmann, A.; Raschke, M. B.; Ernstorfer, R. Nanofocused Plasmon-Driven Sub-10 fs Electron Point Source. *ACS Photonics* **2016**, *3*, 611−619.

(16) Vogelsang, J.; Robin, J.; Nagy, B. J.; Dombi, P.; Rosenkranz, D.; Schiek, M.; Groß, P.; Lienau, C. Ultrafast Electron Emission from a Sharp Metal Nanotaper Driven by Adiabatic Nanofocusing of Surface Plasmons. *Nano Lett.* **2015**, *15*, 4685−4691.

(17) Dombi, P.; Hörl, A.; Rácz, P.; Márton, I.; Trügler, A.; Krenn, J. R.; Hohenester, U. Ultrafast Strong-Field Photoemission from Plasmonic Nanoparticles. *Nano Lett.* **2013**, *13*, 674−678.

(18) Motl, N. E.; Smith, A. F.; DeSantis, C. J.; Skrabalak, S. E. Engineering Plasmonic Metal Colloids through Composition and Structural Design. *Chem. Soc. Rev.* **2014**, *43*, 3823−3834.

(19) Burrows, N. D.; Vartanian, A. M.; Abadeer, N. S.; Grzincic, E. M.; Jacob, L. M.; Lin, W. N.; Li, J.; Dennison, J. M.; Hinman, J. G.; Murphy, C. J. Anisotropic Nanoparticles and Anisotropic Surface Chemistry. *J. Phys. Chem. Lett.* **2016**, *7*, 632−641.

(20) Choo, P.; Arenas-Esteban, D.; Jung, I.; Chang, W. J.; Weiss, E. A.; Bals, S.; Odom, T. W. Investigating Reaction Intermediates During the Seedless Growth of Gold Nanostars Using Electron Tomography. *ACS Nano* **2022**, *16*, 4408−4414.

(21) Mubeen, S.; Lee, J.; Singh, N.; Kramer, S.; Stucky, G. D.; Moskovits, M. An Autonomous Photosynthetic Device in Which All Charge Carriers Derive from Surface Plasmons. *Nat. Nanotechnol.* **2013**, *8*, 247−251.

(22) Hao, F.; Nehl, C. L.; Hafner, J. H.; Nordlander, P. Plasmon Resonances of a Gold Nanostar. *Nano Lett.* **2007**, *7*, 729−732.

(23) Hrelescu, C.; Sau, T. K.; Rogach, A. L.; Jäckel, F.; Laurent, G.; Douillard, L.; Charra, F. Selective Excitation of Individual Plasmonic Hotspots at the Tips of Single Gold Nanostars. *Nano Lett.* **2011**, *11*, 402−407.

(24) Pettine, J.; Grubisic, A.; Nesbitt, D. J. Polarization-Controlled Directional Multiphoton Photoemission from Hot Spots on Single Au Nanoshells. *J. Phys. Chem. C* **2018**, *122*, 14805−14813.

(25) Keathley, P. D.; Putnam, W. P.; Vasireddy, P.; Hobbs, R. G.; Yang, Y.; Berggren, K. K.; Kartner, F. X. Vanishing Carrier-Envelope-Phase-Sensitive Response in Optical-Field Photoemission from Plasmonic Nanoantennas. *Nat. Phys.* **2019**, *15*, 1128−1134.

(26) Wu, K.; Chen, J.; McBride, J. R.; Lian, T. Efficient Hot-Electron Transfer by a Plasmon-Induced Interfacial Charge-Transfer Transition. *Science* **2015**, *349*, 632−635.

(27) Tan, S. J.; Argondizzo, A.; Ren, J. D.; Liu, L. M.; Zhao, J.; Petek, H. Plasmonic Coupling at a Metal/Semiconductor Interface. *Nat. Photonics* **2017**, *11*, 806−812.

(28) Boerigter, C.; Campana, R.; Morabito, M.; Linic, S. Evidence and Implications of Direct Charge Excitation as the Dominant Mechanism in Plasmon-Mediated Photocatalysis. *Nat. Commun.* **2016**, *7*, 10545.

(29) Leenheer, A. J.; Narang, P.; Lewis, N. S.; Atwater, H. A. Solar Energy Conversion Via Hot Electron Internal Photoemission in Metallic Nanostructures: Efficiency Estimates. *J. Appl. Phys.* **2014**, *115*, 134301.

(30) Uskov, A. V.; Protsenko, I. E.; Ikhsanov, R. S.; Babicheva, V. E.; Zhukovsky, S. V.; Lavrinenko, A. V.; O'Reilly, E. P.; Xu, H. X. Internal Photoemission from Plasmonic Nanoparticles: Comparison between Surface and Volume Photoelectric Effects. *Nanoscale* **2014**, *6*, 4716−4727.

(31) Tagliabue, G.; Jermyn, A. S.; Sundararaman, R.; Welch, A. J.; DuChene, J. S.; Pala, R.; Davoyan, A. R.; Narang, P.; Atwater, H. A. Quantifying the Role of Surface Plasmon Excitation and Hot Carrier Transport in Plasmonic Devices. *Nat. Commun.* **2018**, *9*, 3394.

https://doi.org/10.1021/acs.jpcc.2c03425
J. Phys. Chem. C 2022, 126, 14767−14780

(32) Graf, M.; Jalas, D.; Weissmuller, J.; Petrov, A. Y.; Eich, M. Surface-to-Volume Ratio Drives Photoelelectron Injection from Nanoscale Gold into Electrolyte. *ACS Catal.* **2019**, *9*, 3366−3374.
(33) Ikhsanov, R. S.; Novitsky, A. V.; Protsenko, I. E.; Uskov, A. V. Bulk Photoemission from Plasmonic Nanoantennas of Different Shapes. *J. Phys. Chem. C* **2018**, *122*, 11985−11992.
(34) Pettine, J.; Meyer, S. M.; Medeghini, F.; Murphy, C. J.; Nesbitt, D. J. Controlling the Spatial and Momentum Distributions of Plasmonic Carriers: Volume vs Surface Effects. *ACS Nano* **2021**, *15*, 1566−1578.
(35) Medeghini, F.; Pettine, J.; Meyer, S. M.; Murphy, C. J.; Nesbitt, D. J. Regulating and Directionally Controlling Electron Emission from Gold Nanorods with Silica Coatings. *Nano Lett.* **2022**, *22*, 644−651.
(36) Takeyasu, N.; Yamaguchi, K.; Kagawa, R.; Kaneta, T.; Benz, F.; Fujii, M.; Baumberg, J. J. Blocking Hot Electron Emission by SiO_2 Coating Plasmonic Nanostructures. *J. Phys. Chem. C* **2017**, *121*, 18795−18799.
(37) Dubi, Y.; Un, I. W.; Sivan, Y. Thermal Effects - an Alternative Mechanism for Plasmon-Assisted Photocatalysis. *Chem. Sci.* **2020**, *11*, 5017−5027.
(38) Jain, P. K.; Dubi, Y.; Un, I. W.; Sivan, Y. Comment on "Thermal Effects - an Alternative Mechanism for Plasmon-Assisted Photocatalysis". *Chem. Sci.* **2020**, *11*, 9022−9023.
(39) Baffou, G.; Bordacchini, I.; Baldi, A.; Quidant, R. Simple Experimental Procedures to Distinguish Photothermal from Hot-Carrier Processes in Plasmonics. *Light Sci. Appl.* **2020**, *9*, 108.
(40) Feist, A.; et al. Ultrafast Transmission Electron Microscopy Using a Laser-Driven Field Emitter: Femtosecond Resolution with a High Coherence Electron Beam. *Ultramicroscopy* **2017**, *176*, 63−73.
(41) Aidelsburger, M.; Kirchner, F. O.; Krausz, F.; Baum, P. Single-Electron Pulses for Ultrafast Diffraction. *Proc. Natl. Acad. Sci. U.S.A.* **2010**, *107*, 19714−19719.
(42) Müller, M.; Paarmann, A.; Ernstorfer, R. Femtosecond Electrons Probing Currents and Atomic Structure in Nanomaterials. *Nat. Commun.* **2014**, *5*, 5292.
(43) Gulde, M.; Schweda, S.; Storeck, G.; Maiti, M.; Yu, H. K.; Wodtke, A. M.; Schäfer, S.; Ropers, C. Ultrafast Low-Energy Electron Diffraction in Transmission Resolves Polymer/Graphene Superstructure Dynamics. *Science* **2014**, *345*, 200−204.
(44) Vogelgesang, S.; Storeck, G.; Horstmann, J. G.; Diekmann, T.; Sivis, M.; Schramm, S.; Rossnagel, K.; Schäfer, S.; Ropers, C. Phase Ordering of Charge Density Waves Traced by Ultrafast Low-Energy Electron Diffraction. *Nat. Phys.* **2018**, *14*, 184−191.
(45) Polyakov, A.; Senft, C.; Thompson, K. F.; Feng, J.; Cabrini, S.; Schuck, P. J.; Padmore, H. A.; Peppernick, S. J.; Hess, W. P. Plasmon-Enhanced Photocathode for High Brightness and High Repetition Rate X-Ray Sources. *Phys. Rev. Lett.* **2013**, *110*, 076802.
(46) Hobbs, R. G.; Yang, Y.; Fallahi, A.; Keathley, P. D.; De Leo, E.; Kärtner, F. X.; Graves, W. S.; Berggren, K. K. High-Yield, Ultrafast, Surface Plasmon-Enhanced, Au Nanorod Optical Field Electron Emitter Arrays. *ACS Nano* **2014**, *8*, 11474−11482.
(47) Rybka, T.; Ludwig, M.; Schmalz, M. F.; Knittel, V.; Brida, D.; Leitenstorfer, A. Sub-Cycle Optical Phase Control of Nanotunnelling in the Single-Electron Regime. *Nat. Photonics* **2016**, *10*, 667−670.
(48) Yang, Y. J.; Turchetti, M.; Vasireddy, P.; Putnam, W. P.; Karnbach, O.; Nardi, A.; Kartner, F. X.; Berggren, K. K.; Keathley, P. D. Light Phase Detection with on-Chip Petahertz Electronic Networks. *Nat. Commun.* **2020**, *11*, 3407.
(49) Zimmermann, P.; Hötger, A.; Fernandez, N.; Nolinder, A.; Müller, K.; Finley, J. J.; Holleitner, A. W. Toward Plasmonic Tunnel Gaps for Nanoscale Photoemission Currents by on-Chip Laser Ablation. *Nano Lett.* **2019**, *19*, 1172−1178.
(50) Cortes, E.; Xie, W.; Cambiasso, J.; Jermyn, A. S.; Sundararaman, R.; Narang, P.; Schlucker, S.; Maier, S. A. Plasmonic Hot Electron Transport Drives Nano-Localized Chemistry. *Nat. Commun.* **2017**, *8*, 14880.
(51) Wu, B. H.; Liu, D. Y.; Mubeen, S.; Chuong, T. T.; Moskovits, M.; Stucky, G. D. Anisotropic Growth of TiO_2 onto Gold Nanorods for Plasmon-Enhanced Hydrogen Production from Water Reduction. *J. Am. Chem. Soc.* **2016**, *138*, 1114−1117.
(52) Aslam, U.; Rao, V. G.; Chavez, S.; Linic, S. Catalytic Conversion of Solar to Chemical Energy on Plasmonic Metal Nanostructures. *Nat. Catal.* **2018**, *1*, 656−665.
(53) Aeschlimann, M.; Bauer, M.; Bayer, D.; Brixner, T.; García de Abajo, F. J.; Pfeiffer, W.; Rohmer, M.; Spindler, C.; Steeb, F. Adaptive Subwavelength Control of Nano-Optical Fields. *Nature* **2007**, *446*, 301−304.
(54) Ballarotto, V. W.; Breban, M.; Siegrist, K.; Phaneuf, R. J.; Williams, E. D. Photoelectron Emission Microscopy of Ultrathin Oxide Covered Devices. *J. Vac. Sci. Technol. B* **2002**, *20*, 2514−2518.
(55) Linic, S.; Christopher, P.; Ingram, D. B. Plasmonic-Metal Nanostructures for Efficient Conversion of Solar to Chemical Energy. *Nat. Mater.* **2011**, *10*, 911−921.
(56) Tatsuma, T.; Nishi, H.; Ishida, T. Plasmon-Induced Charge Separation: Chemistry and Wide Applications. *Chem. Sci.* **2017**, *8*, 3325−3337.
(57) Wang, F.; Cheng, S.; Bao, Z. H.; Wang, J. F. Anisotropic Overgrowth of Metal Heterostructures Induced by a Site-Selective Silica Coating. *Angew. Chem., Int. Ed.* **2013**, *52*, 10344−10348.
(58) Zhu, X. Z.; Jia, H. L.; Zhu, X. M.; Cheng, S.; Zhuo, X. L.; Qin, F.; Yang, Z.; Wang, J. F. Selective Pd Deposition on Au Nanobipyramids and Pd Site-Dependent Plasmonic Photocatalytic Activity. *Adv. Funct. Mater.* **2017**, *27*, 1700016.
(59) Janicek, B. E.; et al. Quantitative Imaging of Organic Ligand Density on Anisotropic Inorganic Nanocrystals. *Nano Lett.* **2019**, *19*, 6308−6314.
(60) Moskovits, M. The Case for Plasmon-Derived Hot Carrier Devices. *Nat. Nanotechnol.* **2015**, *10*, 6−8.
(61) Choueiri, R. M.; et al. Surface Patterning of Nanoparticles with Polymer Patches. *Nature* **2016**, *538*, 79−83.
(62) Rowe, L. R.; Chapman, B. S.; Tracy, J. B. Understanding and Controlling the Morphology of Silica Shells on Gold Nanorods. *Chem. Mater.* **2018**, *30*, 6249−6258.
(63) Linic, S.; Chavez, S.; Elias, R. Flow and Extraction of Energy and Charge Carriers in Hybrid Plasmonic Nanostructures. *Nat. Mater.* **2021**, *20*, 916−924.
(64) Yang, X. Q. Q.; Lu, Y.; Liu, Y.; Wang, J.; Shao, L.; Wang, J. F. F. Heterostructures Built through Site-Selective Deposition on Anisotropic Plasmonic Metal Nanocrystals and Their Applications. *Small Structures* **2021**, *2*, 2100101.
(65) Szczerbinski, J.; Yin, H.; Zhang, Y. J.; Zhang, F. L.; Li, J. F.; Zenobi, R. Preserving Plasmonic Nanostructures from Laser-Induced Deactivation by a Protective Dielectric Shell. *J. Phys. Chem. C* **2020**, *124*, 6385−6394.
(66) Zhang, T. T.; Zhao, H. Y.; He, S. N.; Liu, K.; Liu, H. Y.; Yin, Y. D.; Gao, C. B. Unconventional Route to Encapsulated Ultrasmall Gold Nanoparticles for High-Temperature Catalysis. *ACS Nano* **2014**, *8*, 7297−7304.
(67) Gao, Z.; Burrows, N. D.; Valley, N. A.; Egger, S.; Schatz, G. C.; Murphy, C. J.; Haynes, C. L. In Solution SERS Sensing Using Mesoporous Silica-Coated Gold Nanorods. *Analyst* **2016**, *141*, 6604−6604.
(68) Jain, P. K.; Qian, W.; El-Sayed, M. A. Ultrafast Cooling of Photoexcited Electrons in Gold Nanoparticle-Thiolated DNA Conjugates Involves the Dissociation of the Gold-Thiol Bond. *J. Am. Chem. Soc.* **2006**, *128*, 2426−2433.
(69) Liao, P. F.; Wokaun, A. Lightning Rod Effect in Surface Enhanced Raman Scattering. *J. Chem. Phys.* **1982**, *76*, 751−752.
(70) Krüger, M.; Lemell, C.; Wachter, G.; Burgdörfer, J.; Hommelhoff, P. Attosecond Physics Phenomena at Nanometric Tips. *J. Phys. B* **2018**, *51*, 172001.
(71) Lombardi, A.; Loumaigne, M.; Crut, A.; Maioli, P.; Del Fatti, N.; Vallee, F.; Spuch-Calvar, M.; Burgin, J.; Majimel, J.; Treguer-Delapierre, M. Surface Plasmon Resonance Properties of Single Elongated Nanoobjects: Gold Nanobipyramids and Nanorods. *Langmuir* **2012**, *28*, 9027−9033.

https://doi.org/10.1021/acs.jpcc.2c03425
J. Phys. Chem. C 2022, 126, 14767−14780

(72) Chikkaraddy, R.; de Nijs, B.; Benz, F.; Barrow, S. J.; Scherman, O. A.; Rosta, E.; Demetriadou, A.; Fox, P.; Hess, O.; Baumberg, J. J. Single-Molecule Strong Coupling at Room Temperature in Plasmonic Nanocavities. *Nature* **2016**, *535*, 127−130.
(73) Ciraci, C.; Hill, R. T.; Mock, J. J.; Urzhumov, Y.; Fernandez-Dominguez, A. I.; Maier, S. A.; Pendry, J. B.; Chilkoti, A.; Smith, D. R. Probing the Ultimate Limits of Plasmonic Enhancement. *Science* **2012**, *337*, 1072−1074.
(74) Schertz, F.; Schmelzeisen, M.; Kreiter, M.; Elmers, H. J.; Schonhense, G. Field Emission of Electrons Generated by the near Field of Strongly Coupled Plasmons. *Phys. Rev. Lett.* **2012**, *108*, 237602.
(75) Hao, E.; Li, S. Y.; Bailey, R. C.; Zou, S. L.; Schatz, G. C.; Hupp, J. T. Optical Properties of Metal Nanoshells. *J. Phys. Chem. B* **2004**, *108*, 1224−1229.
(76) Grubisic, A.; Mukherjee, S.; Halas, N.; Nesbitt, D. J. Anomalously Strong Electric near-Field Enhancements at Defect Sites on Au Nanoshells Observed by Ultrafast Scanning Photoemission Imaging Microscopy. *J. Phys. Chem. C* **2013**, *117*, 22545−22559.
(77) Bormann, R.; Gulde, M.; Weismann, A.; Yalunin, S. V.; Ropers, C. Tip-Enhanced Strong-Field Photoemission. *Phys. Rev. Lett.* **2010**, *105*, 147601.
(78) Marsell, E.; et al. Nanoscale Imaging of Local Few-Femtosecond near-Field Dynamics within a Single Plasmonic Nanoantenna. *Nano Lett.* **2015**, *15*, 6601−6608.
(79) Yalunin, S. V.; Gulde, M.; Ropers, C. Strong-Field Photoemission from Surfaces: Theoretical Approaches. *Phys. Rev. B* **2011**, *84*, 195426.
(80) Feuerbacher, B.; Willis, R. F. Photoemission and Electron States at Clean Surfaces. *J. Phys. C* **1976**, *9*, 169−216.
(81) Makinson, R. E. B. The Surface Photoelectric Effect. *Phys. Rev.* **1949**, *75*, 1908−1911.
(82) Adawi, I. Theory of Surface Photoelectric Effect for One and Two Photons. *Phys. Rev.* **1964**, *134*, 788−798.
(83) Mahan, G. D. Theory of Photoemission in Simple Metals. *Phys. Rev. B* **1970**, *2*, 4334−4350.
(84) Grubisic, A.; Schweikhard, V.; Baker, T. A.; Nesbitt, D. J. Coherent Multiphoton Photoelectron Emission from Single Au Nanorods: The Critical Role of Plasmonic Electric near-Field Enhancement. *ACS Nano* **2013**, *7*, 87−99.
(85) Stockman, M. I. Nanoplasmonics: Past, Present, and Glimpse into Future. *Opt. Express* **2011**, *19*, 22029−22106.
(86) Awada, C.; Popescu, T.; Douillard, L.; Charra, F.; Perron, A.; Yockell-Lelievre, H.; Baudrion, A. L.; Adam, P. M.; Bachelot, R. Selective Excitation of Plasmon Resonances of Single Au Triangles by Polarization-Dependent Light Excitation. *J. Phys. Chem. C* **2012**, *116*, 14591−14598.
(87) Yanagisawa, H.; Hafner, C.; Dona, P.; Klockner, M.; Leuenberger, D.; Greber, T.; Hengsberger, M.; Osterwalder, J. Optical Control of Field-Emission Sites by Femtosecond Laser Pulses. *Phys. Rev. Lett.* **2009**, *103*, 257603.
(88) Aeschlimann, M.; et al. Spatiotemporal Control of Nanooptical Excitations. *Proc. Natl. Acad. Sci. U.S.A.* **2010**, *107*, 5329−5333.
(89) Lehr, M.; Foerster, B.; Schmitt, M.; Krüger, K.; Sönnichsen, C.; Schönhense, G.; Elmers, H. J. Momentum Distribution of Electrons Emitted from Resonantly Excited Individual Gold Nanorods. *Nano Lett.* **2017**, *17*, 6606−6612.
(90) Lehr, M.; Bley, K.; Vogel, N.; Rethfeld, B.; Schönhense, G.; Elmers, H.-J. Evidence of Spatially Inhomogeneous Electron Temperature in a Resonantly Excited Array of Bow-Tie Nanoantennas. *J. Phys. Chem. C* **2019**, *123*, 12429−12436.
(91) Petek, H. Photoexcitation of Adsorbates on Metal Surfaces: One-Step or Three-Step. *J. Chem. Phys.* **2012**, *137*, 091704.
(92) Linic, S.; Aslam, U.; Boerigter, C.; Morabito, M. Photochemical Transformations on Plasmonic Metal Nanoparticles. *Nat. Mater.* **2015**, *14*, 567−576.
(93) Foerster, B.; Hartelt, M.; Collins, S. S. E.; Aeschlimann, M.; Link, S.; Sonnichsen, C. Interfacial States Cause Equal Decay of Plasmons and Hot Electrons at Gold-Metal Oxide Interfaces. *Nano Lett.* **2020**, *20*, 3338−3343.
(94) Tamm, I.; Schubin, S. On the Theory of the Photoelectric Effect in Metals. *Z. Phys.* **1931**, *68*, 97−113.
(95) Glasser, M. L.; Bagchi, A. Theories of Photoemission from Metal Surfaces. *Prog. Surf. Sci.* **1976**, *7*, 113−148.
(96) Miller, T.; McMahon, W. E.; Chiang, T. C. Interference between Bulk and Surface Photoemission Transitions in Ag(111). *Phys. Rev. Lett.* **1996**, *77*, 1167−1170.
(97) Tagliabue, G.; et al. Ultrafast Hot-Hole Injection Modifies Hot-Electron Dynamics in Au/P-GaN Heterostructures. *Nat. Mater.* **2020**, *19*, 1312−1318.
(98) Khurgin, J. B. Hot Carriers Generated by Plasmons: Where Are They Generated and Where Do They Go from There? *Faraday Discuss.* **2019**, *214*, 35−58.
(99) Narang, P.; Sundararaman, R.; Atwater, H. A. Plasmonic Hot Carrier Dynamics in Solid-State and Chemical Systems for Energy Conversion. *Nanophotonics* **2016**, *5*, 96−111.
(100) Govorov, A. O.; Zhang, H.; Gun'ko, Y. K. Theory of Photoinjection of Hot Plasmonic Carriers from Metal Nanostructures into Semiconductors and Surface Molecules. *J. Phys. Chem. C* **2013**, *117*, 16616−16631.
(101) Manjavacas, A.; Liu, J. G.; Kulkarni, V.; Nordlander, P. Plasmon-Induced Hot Carriers in Metallic Nanoparticles. *ACS Nano* **2014**, *8*, 7630−7638.
(102) Brown, A. M.; Sundararaman, R.; Narang, P.; Goddard, W. A.; Atwater, H. A. Nonradiative Plasmon Decay and Hot Carrier Dynamics: Effects of Phonons, Surfaces, and Geometry. *ACS Nano* **2016**, *10*, 957−966.
(103) Khurgin, J. B.; Levy, U. Generating Hot Carriers in Plasmonic Nanoparticles: When Quantization Does Matter? *ACS Photonics* **2020**, *7*, 547−553.
(104) Bainbridge, A. R.; Bryan, W. A. Velocity Map Imaging of Femtosecond Laser Induced Photoelectron Emission from Metal Nanotips. *New J. Phys.* **2014**, *16*, 103031.
(105) Jermyn, A. S.; Tagliabue, G.; Atwater, H. A.; Goddard, W. A.; Narang, P.; Sundararaman, R. Transport of Hot Carriers in Plasmonic Nanostructures. *Phys. Rev. Mater.* **2019**, *3*, 075201.
(106) Pettine, J.; Marton Menendez, A.; Nesbitt, D. J. Continuous Angular Control over Anisotropic Photoemission from Isotropic Gold Nanoshells. *J. Chem. Phys.* **2020**, *153*, 101101.
(107) Berglund, C. N.; Spicer, W. E. Photoemission Studies of Copper and Silver: Theory. *Phys. Rev. A* **1964**, *136*, 1030−1044.
(108) Chen, Q. Y.; Bates, C. W. Geometrical Factors in Enhanced Photoyield from Small Metal Particles. *Phys. Rev. Lett.* **1986**, *57*, 2737−2740.
(109) Stuart, R.; Spicer, W. E.; Wooten, F. Monte Carlo Calculations Pertaining to Transport of Hot Electrons in Metals. *Phys. Rev. A* **1964**, *135*, 495−505.
(110) Blandre, E.; Jalas, D.; Petrov, A. Y.; Eich, M. Limit of Efficiency of Generation of Hot Electrons in Metals and Their Injection inside a Semiconductor Using a Semiclassical Approach. *ACS Photonics* **2018**, *5*, 3613−3620.
(111) Grajower, M.; Levy, U.; Khurgin, J. B. The Role of Surface Roughness in Plasmonic-Assisted Internal Photoemission Schottky Photodetectors. *ACS Photonics* **2018**, *5*, 4030−4036.
(112) Kanter, H. Slow-Electron Mean Free Paths in Aluminum, Silver, and Gold. *Phys. Rev. B* **1970**, *1*, 522−536.
(113) Ladstadter, F.; Hohenester, U.; Puschnig, P.; Ambrosch-Draxl, C. First-Principles Calculation of Hot-Electron Scattering in Metals. *Phys. Rev. B* **2004**, *70*, 235125.
(114) Ratchford, D. C.; Dunkelberger, A. D.; Vurgaftman, I.; Owrutsky, J. C.; Pehrsson, P. E. Quantification of Efficient Plasmonic Hot-Electron Injection in Gold Nanoparticle TiO_2 Films. *Nano Lett.* **2017**, *17*, 6047−6055.
(115) Hobbs, R. G.; Putnam, W. P.; Fallahi, A.; Yang, Y.; Kärtner, F. X.; Berggren, K. K. Mapping Photoemission and Hot-Electron Emission from Plasmonic Nanoantennas. *Nano Lett.* **2017**, *17*, 6069−6076.

https://doi.org/10.1021/acs.jpcc.2c03425
J. Phys. Chem. C 2022, 126, 14767−14780

(116) Merschdorf, M.; Pfeiffer, W.; Thon, A.; Voll, S.; Gerber, G. Photoemission from Multiply Excited Surface Plasmons in Ag Nanoparticles. *Appl. Phys. A: Mater. Sci. Process.* **2000**, *71*, 547−552.
(117) Grubisic, A.; Ringe, E.; Cobley, C. M.; Xia, Y. N.; Marks, L. D.; Van Duyne, R. P.; Nesbitt, D. J. Plasmonic near-Electric Field Enhancement Effects in Ultrafast Photoelectron Emission: Correlated Spatial and Laser Polarization Microscopy Studies of Individual Ag Nanocubes. *Nano Lett.* **2012**, *12*, 4823−4829.
(118) Sivis, M.; Pazos-Perez, N.; Yu, R. W.; Alvarez-Puebla, R.; García de Abajo, F. J.; Ropers, C. Continuous-Wave Multiphoton Photoemission from Plasmonic Nanostars. *Commun. Phys.* **2018**, *1*, 13.
(119) Herink, G.; Solli, D. R.; Gulde, M.; Ropers, C. Field-Driven Photoemission from Nanostructures Quenches the Quiver Motion. *Nature* **2012**, *483*, 190−193.
(120) Dombi, P.; Papa, Z.; Vogelsang, J.; Yalunin, S. V.; Sivis, M.; Herink, G.; Schafer, S.; Gross, P.; Ropers, C.; Lienau, C. Strong-Field Nano-Optics. *Rev. Mod. Phys.* **2020**, *92*, 025003.
(121) Bauer, M.; Marienfeld, A.; Aeschlimann, M. Hot Electron Lifetimes in Metals Probed by Time-Resolved Two-Photon Photoemission. *Prog. Surf. Sci.* **2015**, *90*, 319−376.
(122) Zhukov, V. P.; Chulkov, E. V. The Femtosecond Dynamics of Electrons in Metals. *Phys. Usp.* **2009**, *52*, 105−136.
(123) Quinn, J. J. Range of Excited Electrons in Metals. *Phys. Rev.* **1962**, *126*, 1453−1457.
(124) Aeschlimann, M.; Bauer, M.; Pawlik, S.; Knorren, R.; Bouzerar, G.; Bennemann, K. H. Transport and Dynamics of Optically Excited Electrons in Metals. *Appl. Phys. A: Mater. Sci. Process.* **2000**, *71*, 485−491.
(125) Voisin, C.; Christofilos, D.; Del Fatti, N.; Vallee, F.; Prevel, B.; Cottancin, E.; Lerme, J.; Pellarin, M.; Broyer, M. Size-Dependent Electron-Electron Interactions in Metal Nanoparticles. *Phys. Rev. Lett.* **2000**, *85*, 2200−2203.
(126) Voisin, C.; Christofilos, D.; Loukakos, P. A.; Del Fatti, N.; Vallee, F.; Lerme, J.; Gaudry, M.; Cottancin, E.; Pellarin, M.; Broyer, M. Ultrafast Electron-Electron Scattering and Energy Exchanges in Noble-Metal Nanoparticles. *Phys. Rev. B* **2004**, *69*, 195416.
(127) Merschdorf, M.; Kennerknecht, C.; Pfeiffer, W. Collective and Single-Particle Dynamics in Time-Resolved Two-Photon Photoemission. *Phys. Rev. B* **2004**, *70*, 193401.
(128) Watanabe, K.; Menzel, D.; Nilius, N.; Freund, H. J. Photochemistry on Metal Nanoparticles. *Chem. Rev.* **2006**, *106*, 4301−4320.
(129) Brongersma, M. L.; Halas, N. J.; Nordlander, P. Plasmon-Induced Hot Carrier Science and Technology. *Nat. Nanotechnol.* **2015**, *10*, 25−34.
(130) Pettine, J.; Maioli, P.; Vallee, F.; Del Fatti, N.; Nesbitt, D. J. Energy-Resolved Femtosecond Hot Electron Dynamics in Single Plasmonic Nanoparticles. *arXiv:2207.05319* **2022**, DOI: 10.48550/arXiv.2207.05319.
(131) Pawlik, S.; Bauer, M.; Aeschlimann, M. Lifetime Difference of Photoexcited Electrons between Intraband and Interband Transitions. *Surf. Sci.* **1997**, *377*, 206−209.
(132) Cao, J.; Gao, Y.; Elsayed-Ali, H. E.; Miller, R. J. D.; Mantell, D. A. Femtosecond Photoemission Study of Ultrafast Electron Dynamics in Single-Crystal Au(111) Films. *Phys. Rev. B* **1998**, *58*, 10948−10952.
(133) Link, S.; Burda, C.; Wang, Z. L.; El-Sayed, M. A. Electron Dynamics in Gold and Gold-Silver Alloy Nanoparticles: The Influence of a Nonequilibrium Electron Distribution and the Size Dependence of the Electron-Phonon Relaxation. *J. Chem. Phys.* **1999**, *111*, 1255−1264.
(134) Hartland, G. V. Optical Studies of Dynamics in Noble Metal Nanostructures. *Chem. Rev.* **2011**, *111*, 3858−3887.
(135) Boerigter, C.; Aslam, U.; Linic, S. Mechanism of Charge Transfer from Plasmonic Nanostructures to Chemically Attached Materials. *ACS Nano* **2016**, *10*, 6108−6115.
(136) Fann, W. S.; Storz, R.; Tom, H. W. K.; Bokor, J. Electron Thermalization in Gold. *Phys. Rev. B* **1992**, *46*, 13592−13595.

https://doi.org/10.1021/acs.jpcc.2c03425
J. Phys. Chem. C 2022, 126, 14767−14780